Received 19 December 2023; revised 17 January 2024; accepted 27 January 2024. Date of publication 8 February 2024; date of current version 26 March 2024.

Digital Object Identifier 10.1109/OJAP.2024.3363730

Kriging Methodology for Uncertainty Quantification in Computational Electromagnetics

STEPHEN KASDORF (Student Member, IEEE), JAKE J. HARMON (Member, IEEE), AND BRANISLAV M. NOTAROŠ (Fellow, IEEE)

Department of Electrical and Computer Engineering, Colorado State University, Fort Collins, CO 80523, USA

CORRESPONDING AUTHOR: B. M. NOTAROŠ (e-mail: notaros@colostate.edu)

This work was supported in part by the U.S. Air Force Research Laboratory under Contract FA8650-20-C-1132.

This article has supplementary downloadable material available at https://doi.org/10.1109/OJAP.2023.3363730, provided by the authors.

ABSTRACT We present the implementation and use of the Kriging methodology, i.e., surrogate models based on Kriging interpolation, in uncertainty quantification (UQ) in computational electromagnetics (CEM). We provide consistent, unified, and comprehensive description, derivation, implementation, use, validation, and comparative study of accuracy and convergence of several advanced Kriging approaches, namely, the universal Kriging, Taylor Kriging, and gradient-enhanced Kriging methods, for reconstruction of probability-density function in UQ CEM problems. We also propose, derive, and demonstrate the gradient-enhanced Taylor Kriging (GETK) methodology, novel to science and engineering in general. Numerical results using higher-order finite-element scattering modeling show that Kriging methods for UQ in CEM are able to accurately output probability-density function prediction for a quantity of interest (e.g., radar cross-section) given the probability density of stochastic input parameters (e.g., material uncertainties), as very efficient alternatives to Monte Carlo simulations. The novel GETK method shows dramatic enhancement over all other tested approaches, Kriging and non-Kriging, in terms of surrogate function accuracy and convergence with increasing the number of sample (training) points in all examples.

INDEX TERMS Adjoints, computational electromagnetics, finite element method, gradient-enhanced Kriging methods, Kriging, material uncertainty, maximum likelihood estimation, metamodel, scattering, surrogate models, uncertainty quantification.

I. INTRODUCTION

AMONG the most important topics in computational science and engineering, and particularly so in computational electromagnetics (CEM), uncertainty quantification (UQ) is at the forefront of research due to the far-ranging academic and industrial uses [1]. Through effective and rigorous UQ, the quality of analyses and designs may be improved drastically, both in terms of effectiveness and reliability. Indeed, from the position of satellites to the manufacture of the simplest resistor or tomorrow's weather, uncertainty is unavoidable. Further, uncertainty is essential in CEM as material parameters of an antenna/scatterer, object shape/size, mutual positions/ orientations, etc. are all uncertain input parameters, which may be known only within a specific tolerance. UQ in CEM involves studies of how the input parameter uncertainty translates into uncertainty in the generated electric or magnetic field, for example, where the UQ-CEM aims at assessing the sensitivity of the field to the uncertain input parameter. Troublesome sources of uncertainty also include experimental uncertainty, inadequacy and randomness of a model or some of its components, discretization error, and other sources of numerical error, e.g., numerical integration and finite-precision arithmetic.

In CEM, the finite element method and the method of moments, along with similar alternatives such as finite difference methods, provide the underlying model for solving the relevant partial differential equation or integral equation problems and therefore the structure by which the uncertainty influences or perturbs the solution and the quantities of interest (QoIs) computed from the solution. Namely, in practical applications, we are often interested in specific QoIs (i.e., functionals of the solution). With the solution

itself being a random quantity, by tailoring results to the set of necessary computables, the parameter space may be explored more effectively, driving higher quality UQ analysis for the goal-oriented simulation objectives and the same or lower computational cost. For a waveguide structure, a typical QoI that we are interested in studying could be the cutoff frequency or the propagation coefficient; for a scattering target, the QoI could be the radar cross section (RCS) or a specific component of the scattered field. In other words, according to our goal-oriented approach, rather than the solution directly, our primary objective is the study of a goal functional (or a collection of goal functionals) [2], [3]. The general UQ problem we are considering in this work can be formulated as predicting and quantifying the probability density function of a QoI in a CEM simulation given the probability density of uncertain (stochastic) input parameters to the CEM structure and model.

Traditional Monte Carlo methods – the conventional and dominant approach to UQ – are straightforward, nonintrusive (the deterministic forward solver can be used as a "black box" and only postprocessing needs to be done on simulation results), and can easily be applied to higher-dimensional parameter spaces [4], [5], [6]. However, the number of samples required restricts applicability to low-cost computations or when high-precision UQ is not needed, as the convergence of Monte Carlo simulation is proportional to the square root of the number of samples. For example, in [7], [8], [9], standard Monte Carlo methods were applied to rough surface scattering. Given the precision required of modern devices and objectives, simulations require similar resolution, demanding more expensive computational models. Hence, when model complexity and precision require a large number of unknowns (degrees of freedom), each Monte Carlo solve can take large (often prohibitive) computation time. Thousands (or many more) of points are usually required for Monte Carlo convergence, which makes this simulation practically unattainable in many cases.

Given the potential unsuitability of standard Monte Carlo methods, then, a significant body of research has been devoted to stochastic spectral Galerkin approaches, e.g., polynomial chaos expansion (PCE) [10], [11], [12], [13], [14], [15], [16], [17], and stochastic collocation approaches [18], [19], [20], [21], [22], [23], [24]. Some of these methods are intrusive techniques, requiring substantial modifications to the deterministic CEM solver and thus being undesirable due to the implementation complexity required. Some methods suffer the curse of dimensionality, i.e., the rate of convergence deteriorates with the increase of dimension of the parameter space), an important issue in UQ that is not addressed in this work, nor we discuss ways of its mitigation.

Additionally, with the increasing involvement of machine learning and optimization techniques in engineering projects, robust and automated uncertainty quantification is of vital importance. Recently, given the necessity to consider uncertainty as outlined above, researchers and practitioners in design optimization have begun to consider uncertainty as an integral component of the applied procedures. For instance, as outlined in [25], [26], [27], [28], UQ-augmented machine learning techniques for optimizing designs in electromagnetics have resulted in substantial improvements for real-world applications. While promising, in most cases, these techniques rely on standard Monte Carlo methods, therefore suffering the same weaknesses hampering other areas of engineering and numerical methods.

In recent years, sensitivity analysis and optimization methods have been increasingly based on surrogate models primarily due to the reduced computational cost when compared with Monte Carlo methods. Surrogate models replace expensive function evaluations with an analytical model which is constructed using samples of the physical (original) simulation (on the actual model) [6], [29], [30]. If at some point the surrogate evaluations become sufficiently accurate when compared to the actual (physical) model, the surrogate can now be used instead of the prohibitively expensive function evaluations. Several surrogate models, such as the least square polynomial, multi-layer perceptron, radial basis function, and Kriging models and methods were examined in [31], and Kriging and radial basis function methods showed the most promise.

This paper presents the implementation and use of the Kriging methodology, i.e., surrogate models based on Kriging interpolation, also referred to as Gaussian process regression, in UQ in CEM. Kriging methods have been applied in optimization and UQ problems in other fields of science and engineering, such as aeronautics, aerospace, geostatistics, fluid dynamics, etc. [6], [29], [30], [31], [32], [33], [34], [35] as well as in optimization of designs in magnetics [36] and CEM [37], [38], [39], [40], [41]. In particular, [37] proposes a combination of the universal Kriging with DIRECT algorithm to increase the accuracy of the surrogate reconstruction by selecting optimum points and using the surrogate model to optimize the size of a slot-array frequency selective surface. In [38], the combination of domain confinement with gradient enhanced ordinary nested Kriging is proposed to reduce the size of the domain of interest in the surrogate reconstruction within the optimization of the parameters of an antenna. Further applications of Kriging interpolation to antenna optimization are presented in [39], [40], [41]. In addition, notable examples of UQ of electronic circuits using Kriging surrogate models and SPICE circuit solvers are given in [42], [43].

We present consistent and unified description, derivation, implementation, and use of several advanced Kriging approaches, namely, the universal Kriging, Taylor Kriging, and gradient-enhanced Kriging methods, for reconstruction of probability density function in CEM problems. We provide in-depth and comprehensive description of Kriging and the necessary methods to calculate covariance, adjoints, correlation, etc. Here, the universal Kriging (UK) is a surrogate method that is advanced from the ordinary Kriging (OK) by the use of basis functions in the form of (typically) power functions in the construction of the Kriging predictor.

The Taylor Kriging (TK) method is a further advancement by means of Taylor series polynomial basis functions centered at the average of sample points. The gradient-enhanced Kriging (GEK) formulation uses gradient values to advance the accuracy of the ordinary Kriging approach. Note that some preliminary results using one of these techniques (TK) are presented in a summary form in [44].

Moreover, this paper proposes a completely new Kriging methodology, the gradient-enhanced Taylor Kriging (GETK) technique. Namely, gradient enhancements as shown in [29], [30], [32], [45] have all been proposed and built on the foundation of the ordinary Kriging method which has no basis functions involved with the regression scheme. In addition, GEK has been implemented in [29] and [32] specifically in the context of UQ and optimization, and was shown to be significantly more accurate than even advanced versions of Kriging such as UK. In this work, we propose, derive (using optimization principles), develop, test, and demonstrate a GEK methodology based on the TK approach which has been shown to generally be the most accurate form of non-gradient-enhanced Kriging methods. The novel GETK methodology has the advantage of making use of gradient information, such as with the GEK method, and basis functions, much like in the UK and TK formulations (and more similarly to TK as we use Taylor series bases). The proposed GETK methodology is novel not only to UQ in CEM but to science and engineering in general, and not only to UQ and general numerical analysis but to all possible uses of Kriging interpolations, of which there are many indeed.

Furthermore, for gradient enhanced surrogate functions in this work, i.e., the GEK and GETK models, the gradients are calculated using our adjoint CEM methodology [2], [3], [46], [47], [48], [49], that is, the gradients are obtained from the suitable adjoint problem that relates the deterministic forward problem to a specific QoI. The benefit of using adjoints to solve for gradients is that the solution requires exactly (only) one additional simulation solve regardless of the dimensionality of the parameter space. Note that adjoint solutions have become increasingly popular in computational methods in general in recent years due to their excellent scaling. Computational thrift is achieved through a goal-oriented focus, with the method built around user-specified quantities of interest.

The paper presents validation and comparative numerical studies of different Kriging methodologies for UQ CEM analysis. We compare and discuss OK, UK, TK, GEK, and GETK solutions to UQ scattering problems and examine the accuracy and convergence of the solution and performance of various approaches when reconstructing an output probability density function given an input probability density from some uncertain quantity, with emphasis on predicting material uncertainty impact on finite element method (FEM) RCS computations. We also validate, evaluate, and discuss the accuracy of various Kriging methods against two well-established non-Kriging UQ approaches. The first is the general adjoint-based gradient-enhanced higher-order parameter sampling (HOPS) UQ methodology [2], [3]. The second is a PCE approach, the arbitrary polynomial chaos (aPC) technique, which is nonintrusive and has been shown to work rather well for UQ elsewhere in applied mathematics [50]. Numerical results show that Kriging methods provide excellent and very useful tools to construct surrogate functions in UQ CEM simulations, with very small numbers of input sample points, as a very efficient alternative to Monte Carlo computations. The results also demonstrate that the novel GETK method outperforms all other approaches, Kriging and non-Kriging, by much faster convergence with increasing the number of sample points and dramatically more accurate probability density reconstruction in all examples.

II. GENERAL PRINCIPLES

A. THE KRIGING SYSTEM

To introduce and explain the principles that all Kriging interpolation methods share and establish the Kriging system of equations in general terms, consider a stochastic function of the following form, which may represent the scattered field based on some input $\mathbf{X}$ [33], [36], [51],

$$Z(\boldsymbol{X}) = \mu(\boldsymbol{X}) + \varepsilon(\boldsymbol{X}), \tag{1}$$

where $\mathbf{X}$ is referred to as a position vector in the parameter space, $\mu(\boldsymbol{X})$ is a mean or drift function, and $\varepsilon(\boldsymbol{X})$ is a random error term with the expected value $E[\varepsilon(\boldsymbol{X})] = 0$. With N observed values, $Z(\boldsymbol{X_1})$, $Z(\boldsymbol{X_2}), \ldots, Z(\boldsymbol{X_N})$, the Kriging predictor, $\widehat{Z}(\boldsymbol{X})$, is given as a linear sum of these values multiplied by unknown weights (λ),

$$\widehat{Z}(\boldsymbol{X}) = \sum_{i=1}^{N} \lambda_i \cdot Z(\boldsymbol{X_i}), \tag{2}$$

where, generally, the hatted, $\widehat{(\cdot)}$, symbology is used to indicate an estimated or predicted quantity value instead of the true value. The weights λ_i are selected based on two conditions combined [51]. Firstly, $\widehat{Z}(\boldsymbol{X})$ is the unbiased estimator of $Z(\boldsymbol{X})$, that is, $E[Z(\boldsymbol{X})] = E[\widehat{Z}(\boldsymbol{X})]$. Secondly, the variance of the estimator error, $Var[\widehat{Z}(\boldsymbol{X}) - Z(\boldsymbol{X})] = Var[\epsilon(\boldsymbol{X})]$, is minimized, which can be expanded into the following expression:

$$\text{Minimize} : Var[\epsilon(\boldsymbol{X})] = \sum_{i=1}^{N} \lambda_i \sum_{j=1}^{N} \lambda_j Cov\big[Z(\boldsymbol{X}_i),\ Z(\boldsymbol{X}_j)\big] - 2\sum_{i=1}^{N} \lambda_i Cov[Z(\boldsymbol{X}_i),\ Z(\boldsymbol{X})] + Var[Z(\boldsymbol{X})] \tag{3}$$

where $Cov[Z(\boldsymbol{X}_i),\ Z(\boldsymbol{X}_j)]$ is the covariance between samples $Z(\boldsymbol{X}_i)$ and $Z(\boldsymbol{X}_j)$, at input sample points $\boldsymbol{X}_i$ and $\boldsymbol{X}_j$ (also referred to as training points), the total number of which is N, and $\widehat{Z}(\boldsymbol{X})$ is the surrogate output reconstruction point. From the first requirement, we take the expected value of (2) and

use the assumption that $E[Z(\boldsymbol{X})] = \mu(\boldsymbol{X})$, i.e., a stationary process, to come up with the Kriging system constraint

$$\mu(\boldsymbol{X}) = \sum_{i=1}^{N} \lambda_i \ \cdot \mu(\boldsymbol{X}_i). \tag{4}$$

In the case of ordinary Kriging, $\mu(\boldsymbol{X})$ is assumed to be constant, yielding the OK system constraint as follows:

$$\sum_{i=1}^{N} \lambda_i = 1. \tag{5}$$

On the other hand, in advanced Kriging approaches, this assumption is abandoned; namely, in the universal Kriging, Taylor Kriging, and gradient-enhanced Taylor Kriging methods, rather than a constant, we instead assume that $\mu(\boldsymbol{X})$ can be expressed as a sum of basis functions up to order M,

$$\mu(\boldsymbol{X}) = \widehat{\boldsymbol{a}}^{\boldsymbol{T}} \boldsymbol{b}(\boldsymbol{X}) = \sum_{l=0}^{M} \widehat{\boldsymbol{a}}_l b_l(\boldsymbol{X}), \tag{6}$$

where $b_l(\boldsymbol{X})$ are basis functions and $\widehat{\boldsymbol{a}}_l$ are unknown coefficients. Thus (4) can be expressed as follows:

$$b_l(\boldsymbol{X}) = \sum_{i=1}^{N} \boldsymbol{\lambda}_i b_l(\boldsymbol{X_i}), \ l = 0, 1, \ldots, M. \tag{7}$$

B. EMPIRICAL COVARIANCE FUNCTION

Having specified the Kriging mean, we now outline the covariance function. We consider two modalities: one based on an empirical covariance function and the other on maximum likelihood estimation (MLE) [29], [32], [36], [52], [53]. The covariance used in Kriging is typically assumed to be homogenous and isotropic [51], meaning that two points in the parameter space have the same covariance if the distance between them is equal and covariance is independent of direction. This allows for the construction of a covariance function $C(h)$ that can be evaluated for any pair of $Z(\boldsymbol{X}_i)$ and $Z(\boldsymbol{X}_j)$, where $h = |\boldsymbol{X}_i - \boldsymbol{X}_j|$ is the Euclidean norm. Note that anisotropic covariance functions, where the function is no longer independent of direction within the input parameter space, can also be included. While this can improve performance in specific scenarios where data correlation trends appear in specific directions, isotropic covariance functions, especially the squared exponential kernel, are typically chosen due to generally good performance in vast majority of scenarios as well as flexibility and ease of use.

In the empirical approach, the distances are separated into discrete bins with every pair of samples used for the Kriging system being placed into one of these bins with $N(h)$ representing the number of sample points that fall within a given bin, and an empirical covariance function is evaluated as [52], [53]

$$C(h) = \frac{1}{|N(h)|} \sum_{(i,j) \in N(h)} Z(\boldsymbol{X_i}) \cdot Z(\boldsymbol{X_{i+h}}) - \ m_i \cdot m_{i+h}. \tag{8}$$

Here, m_i is the mean of function values at distance h given by

$$m_i = \frac{1}{|N(h)|} \sum_{i \in N(h)} Z(\boldsymbol{X}_i). \tag{9}$$

Once the empirical covariance function is created, it is fitted according to one of several models, including Gaussian, exponential, cubic, and spherical among others. The commonly used Gaussian fit function is given by

$$C(h) = C_0 e^{-\left(\frac{h}{d}\right)^2}, \tag{10}$$

where C_0 and d are hyperparameters to be fitted.

C. MAXIMUM LIKELIHOOD ESTIMATION

Within the MLE approach, rather than constructing an empirical function, we instead aim to maximize a likelihood function given the observed data, namely, to make the likelihood function the most likely realization of the data as in a Bayesian approach. The likelihood is given by

$$L(\theta) = \prod_{d=1}^{D} f(X_d|\theta_d), \tag{11}$$

where $f(\cdot)$ is the probability distribution of the data, $\boldsymbol{X}$ is the input vector, whose dimension is D, and $\boldsymbol{\theta}$ is the vector of hyperparameters to be optimized via MLE. However, the likelihood function is difficult to optimize directly, and instead we use the log-likelihood function, i.e., the logarithm of the likelihood function,

$$\begin{aligned} LL(\theta) &= logL(\theta) = log \prod_{k=1}^{D} f(X_k|\theta_d) \\ &= \sum_{k=1}^{D} \log f(X_k|\theta_d). \end{aligned} \tag{12}$$

Given that the logarithm function is monotonic (always increasing), the hyperparameter that maximizes the likelihood function will also maximize the log-likelihood function, and the computational benefit from invoking the log-likelihood becomes evident at higher dimensions, where we turn the multiplication into a summation that can be independently optimized. Additionally, many probability distributions involve exponential functions, which are cancelled by the logarithm function.

The log-likelihood function considered in this work represents a Gaussian prior distribution likelihood given by

$$\begin{aligned} &LL(\theta) \\ &= -\sum_{k=1}^{D} \left[\log\left(2\pi\widehat{\sigma}^2\right)^{\frac{N}{2}} \sqrt{|\boldsymbol{R}|} - \frac{(\boldsymbol{z} - \boldsymbol{B}\widehat{\boldsymbol{a}})^T \boldsymbol{R}^{-1} (\boldsymbol{z} - \boldsymbol{B}\widehat{\boldsymbol{a}})}{2\widehat{\sigma}^2} \right], \end{aligned} \tag{13}$$

where $\boldsymbol{z}$ is a vector of observed data, $\boldsymbol{B}$ is a matrix of basis functions, $\widehat{\sigma}^2$ is the variance of the data, and $\widehat{\boldsymbol{a}}$ are the regression coefficients. $\boldsymbol{R}$ is a correlation function adopted as

$$R\left(\boldsymbol{X}_i, \ \boldsymbol{X}_j, \ \theta\right) = e^{-\theta(X_i - X_j)^2}, \tag{14}$$

and the covariance function is obtained as

$$Cov\big[Z(\boldsymbol{X}_i),\ Z(\boldsymbol{X}_j)\big] = \sigma^2 R\big(\boldsymbol{X}_i, \boldsymbol{X}_j,\ \theta\big). \tag{15}$$

While there are many possible choices for the correlation function, the Kriging systems solutions presented in this paper will all use the Gaussian (squared exponential) correlation function given in (14).

Maximizing (13) represents an MLE set of D nonlinear optimization problems, with D standing for the dimension of the parameter space in (11). To solve the optimization problems, we use derivatives of (13) with respect to $\widehat{\boldsymbol{a}}$ and $\widehat{\sigma}^2$, respectively, leading to

$$\widehat{\boldsymbol{a}} = \left(\boldsymbol{B}^T\boldsymbol{R}^{-1}\boldsymbol{B}\right)^{-1}\boldsymbol{B}^T\boldsymbol{R}^{-1}z \tag{16}$$

$$\widehat{\sigma}^2 = \frac{(z-\boldsymbol{B}\widehat{\boldsymbol{a}})^T R^{-1}(z-\boldsymbol{B}\widehat{\boldsymbol{a}})}{n}. \tag{17}$$

Substituting these expressions back into (13), we perform the optimization as follows:

$$Maximize:\ -\frac{\left[N log\widehat{\sigma}^2 + log|\boldsymbol{R}|\right]}{2}. \tag{18}$$

This regression scheme is calculated using generalized least squares (GLS), since GLS also requires a covariance matrix for regression solution.

D. ADJOINT SOLUTION

For gradient enhanced Kriging models in this work, the gradients are obtained from the suitable adjoint problem [2], [3], [46], [47], [48], [49], where the solution does not suffer from the curse of dimensionality, meaning it requires one additional simulation solve for any number of uncertain input parameters to solve for all gradients. Here we present the solution to the adjoint problem in more general terms, so that the result can be used for alternate choices of QoI if desired. Then we narrow this adjoint solution to extract the gradient specifically for material parameters, which is directly applicable to the material parameter uncertainty as a specific focus of this work.

For clarity with the numerical results section (though other partial differential equations may be treated similarly), we start with the double-curl wave equation to solve for the scattered electric field ($\boldsymbol{E}^{sc}$):

$$\begin{aligned}&\nabla\times\mu_r^{-1}\nabla\times\boldsymbol{E}^{sc} - k_0^2\varepsilon_r\boldsymbol{E}^{sc}\\ &\quad= -\nabla\times\mu_r^{-1}\nabla\times\boldsymbol{E}^{\text{inc}} + k_0^2\varepsilon_r\boldsymbol{E}^{\text{inc}},\end{aligned} \tag{19}$$

where ε_r and μ_r are the relative permittivity and permeability, respectively, of the medium and k_0 is the free space wave number, which we recast using a linear operator, $\mathcal{L}$, and the corresponding excitation function $\boldsymbol{G}$,

$$\mathcal{L}\boldsymbol{E}^{sc} = \mathbf{G}. \tag{20}$$

The adjoint operator, $\mathcal{L}^*$, is defined using the Lagrange identity [54],

$$\langle\mathcal{L}\boldsymbol{u},\ \boldsymbol{v}\rangle = \langle\boldsymbol{u},\ \mathcal{L}^*\boldsymbol{v}\ \rangle, \tag{21}$$

where $\langle\cdot,\cdot\rangle$ denotes the standard L^2 inner-product.

We consider a linear functional J of the forward solution for $\boldsymbol{E}^{sc}$ as the QoI [2],

$$J\big[\boldsymbol{E}^{sc}\big] = \langle\boldsymbol{E}^{\boldsymbol{sc}}, \boldsymbol{p}\rangle, \tag{22}$$

where $\boldsymbol{p}$ is the excitation to the adjoint problem as defined by $\mathcal{L}^*\boldsymbol{v} = \boldsymbol{p}$. The choice of $\boldsymbol{p}$ can be modified for different choices of QoI, and $\boldsymbol{v}$ is the respective solution to the adjoint problem. Following [2], if we then perturb some component of the forward problem, a perturbed forward problem is expressed as

$$\widetilde{\mathcal{L}}\widetilde{\boldsymbol{E}}^{sc} = \widetilde{\boldsymbol{G}}, \tag{23}$$

where $\widetilde{\boldsymbol{E}}^{sc}$ is the perturbed solution with respect to the deterministic reference forward solution, $\boldsymbol{E}^{sc} = \boldsymbol{E}^{ref}$,

$$\widetilde{\boldsymbol{E}}^{sc} = \boldsymbol{E}^{ref} + \delta\boldsymbol{E}^{ref}, \tag{24}$$

with δ standing for a linear operator that signifies the effects of the perturbation, $\widetilde{\mathcal{L}} = \mathcal{L}+\delta\mathcal{L}$, and similarly for $\widetilde{\boldsymbol{G}}$. Taking the inner product of (23) with the adjoint solution $\boldsymbol{v}$ and applying the Lagrange identity,

$$\left\langle\widetilde{\boldsymbol{E}}^{sc}, \boldsymbol{p}\right\rangle = \langle\boldsymbol{E}^{sc}, \boldsymbol{p}\rangle + \left\langle\delta\,\boldsymbol{G} - \delta\mathcal{L}\widetilde{\boldsymbol{E}}^{sc}, \boldsymbol{v}\right\rangle. \tag{25}$$

In a practical case of relatively small perturbations, we apply the definition of the QoI in (24) to obtain

$$J\left[\widetilde{\boldsymbol{E}}^{sc}\right] \approx J\left[\boldsymbol{E}^{ref}\right] + \left\langle\delta\boldsymbol{G} - \delta\mathcal{L}\boldsymbol{E}^{ref}, \boldsymbol{v}\right\rangle. \tag{26}$$

We focus now on the perturbation on the material parameters, say on the reference relative permittivity of a scatterer, $\varepsilon_r = \varepsilon_r^{ref}$, and a perturbation of $\Delta\varepsilon_r = \widetilde{\varepsilon_r} - \varepsilon_r^{ref}$. The effects of the perturbation $\delta\mathcal{L}\boldsymbol{E}^{ref}$ and$\delta\boldsymbol{G}$ are calculated by taking a derivative of the left- and right-hand side of (19), respectively, with respect to the perturbed parameter and multiplying it by the perturbation. Substituting these effects into (26), we arrive at

$$J\left[\widetilde{\boldsymbol{E}}^{sc}\right] \approx\ J\left[\boldsymbol{E}^{ref}\right] + k_0^2\left\langle\left(\boldsymbol{E}^{\boldsymbol{inc}} - \boldsymbol{E}^{ref}\right)\ \Delta\varepsilon_r,\ \boldsymbol{v}\right\rangle. \tag{27}$$

In the case of multiple quantities being perturbed, the perturbation becomes a vector, and the terms $\delta\mathcal{L}\boldsymbol{E}^{ref}$ and $\delta\boldsymbol{G}$ acquire matrix form. If we represent (27) in the form of a first order Taylor series expansion,

$$J\left[\widetilde{\boldsymbol{E}}^{sc}\right] \approx\ J\left[\boldsymbol{E}^{ref}\right] + \Delta\varepsilon_r\ \nabla\ \mathrm{J}\left[\boldsymbol{E}^{ref}\right], \tag{28}$$

we can extract the gradient term, namely, the following expression for the gradient of the QoI:

$$\nabla J\left[\boldsymbol{E}^{ref}\right] = k_0^2\left\langle\boldsymbol{E}^{inc} - \boldsymbol{E}^{ref}, \boldsymbol{v}\right\rangle, \tag{29}$$

to be used in our GEK and GETK methods in this work. Importantly, we can implement this result into computation of any gradient enhanced surrogate function, with a requirement of only one additional simulation solution solve.

III. KRIGING SYSTEM SOLUTIONS

A. UNIVERSAL KRIGING

The variance of the estimator in the universal Kriging (UK) method is given by (3), subject to (7), where basis functions ($\boldsymbol{b}$) are introduced as an advancement over the ordinary Kriging (OK). This can easily be transformed into an unconstrained optimization problem using Lagrange multipliers (δ_l), leading to [33], [36], [51]:

Minimize:

$$\sum_{i=1}^{N}\lambda_i\sum_{j=1}^{N}\lambda_j Cov\big[Z(\boldsymbol{X}_i),\ Z(\boldsymbol{X}_j)\big]-2\sum_{i=1}^{N}\lambda_i Cov[Z(\boldsymbol{X}_i),\ Z(\boldsymbol{X})]$$
$$+\,Var[Z(\boldsymbol{X})]+2\sum_{l=1}^{M}\delta_l\left[\sum_{i=1}^{N}\lambda_i b_l(\boldsymbol{X}_i-b_l(\boldsymbol{X})\right]$$
$$+\,Var\left(Z(\boldsymbol{X})+2\sum_{l=1}^{M}\delta_l\left[\sum_{i=1}^{N}\lambda_i b_l(\boldsymbol{X}_i-b_l(\boldsymbol{X})\right]\right) \tag{30}$$

Taking partial derivatives with respect to λ_i and δ_l, we come up with the following system of matrix equations that can be solved for λ values:

$$\begin{bmatrix}\boldsymbol{\lambda}\\ \boldsymbol{\delta}\end{bmatrix}=\begin{bmatrix}\boldsymbol{C} & \boldsymbol{B}\\ \boldsymbol{B}^T & \boldsymbol{0}\end{bmatrix}^{-1}\begin{bmatrix}\boldsymbol{c}_{x_i x}\\ \boldsymbol{b}_x\end{bmatrix}, \tag{31}$$

$$\boldsymbol{C}=\begin{bmatrix}C_{x_1x_1} & \cdots & C_{x_1x_N}\\ \vdots & \ddots & \vdots\\ C_{x_Nx_1} & \cdots & C_{x_Nx_N}\end{bmatrix}, \tag{32}$$

$$\boldsymbol{B}=\begin{bmatrix}\boldsymbol{b_1}(\boldsymbol{X}_1) & \cdots & \boldsymbol{b}_M(\boldsymbol{X_1})\\ \vdots & \ddots & \vdots\\ \boldsymbol{b}_1(\boldsymbol{X_N}) & \cdots & \boldsymbol{b}_M(\boldsymbol{X_N})\end{bmatrix}. \tag{33}$$

$\boldsymbol{C}$ is a covariance matrix, where $C_{x_ix_j}$ is the covariance between $Z(\boldsymbol{X}_i)$ and $Z(\boldsymbol{X}_j)$ and $\boldsymbol{c}_{x_ix}$ is a vector of covariances evaluated between $Z(\boldsymbol{X_i})$ and $Z(\boldsymbol{X})$, $\boldsymbol{B}$ is a basis function matrix, and $\boldsymbol{b}_x$ represents a vector of basis functions evaluated at $\mathbf{X}$.

In the UK technique, the basis functions are given by

$$b_l(\boldsymbol{X})=\boldsymbol{X}^l,\ \ l=0,\ \ 1,\ldots,M, \tag{34}$$

where the number of basis functions, M, is limited by the following expression involving the dimension of the parameter space, D, and the number of input sample (training) points, N [36], [55]:

$$\frac{(D+M)!}{M!D!}\leq \mathrm{N}. \tag{35}$$

With all the details above, the UK system of equations in (31) is solved, and the computed weights λ_i are used to construct the Kriging predictor $\widehat{Z}(\boldsymbol{X})$ in (2).

B. TAYLOR KRIGING

The Taylor Kriging (TK) methodology is an advancement of the UK technique by means of special Taylor series polynomial basis functions, instead of the power functions in (34), that are adjusted to be more sensitive to sample points, namely, they are centered at the average of sample points. The M^{th} order Taylor series expansion of the mean about $\boldsymbol{X}_0$, where $\boldsymbol{X}_0$ is the average of all sample inputs, is given by [51]

$$\mu(\boldsymbol{X})=\widehat{\boldsymbol{a}}^{\boldsymbol{T}}\boldsymbol{b}(\boldsymbol{X})=\mu(\boldsymbol{X_0})+\mu^{(1)}(\boldsymbol{X_0})(\boldsymbol{X}-\boldsymbol{X_0})$$
$$+\ldots+\frac{\mu^{(\boldsymbol{M})}(\boldsymbol{X_0})(\boldsymbol{X}-\boldsymbol{X_0})^{\boldsymbol{M}}}{\boldsymbol{K!}} \tag{36}$$

With reference to (6), the choices for $b_l(\boldsymbol{X})$ and $\boldsymbol{a}$ in (36) are

$$b_l(\boldsymbol{X})=(\boldsymbol{X}-\boldsymbol{X_0})^{\boldsymbol{l}},\ \ a_l=\mu(\boldsymbol{X_0})^{(\boldsymbol{l})},\ \ l=0,1,\ldots,M. \tag{37}$$

C. GRADIENT ENHANCED KRIGING

As another advancement of the OK method, the gradient-enhanced Kriging (GEK) formulation [29], [30], [32], [45], which uses gradient values to enhance the accuracy of the method, results in the following Kriging matrix equation [30]:

$$\begin{bmatrix}\boldsymbol{\lambda}\\ \widetilde{\boldsymbol{\delta}}\end{bmatrix}=\begin{bmatrix}\dot{\boldsymbol{C}} & \boldsymbol{F}\\ \boldsymbol{F}^T & \boldsymbol{0}\end{bmatrix}^{-1}\begin{bmatrix}\boldsymbol{c}_{x_ix}\\ \boldsymbol{1}\end{bmatrix} \tag{38}$$

Here, $\dot{\boldsymbol{C}}$ is a composite matrix of the covariance matrix in (32) and its derivatives, of size $N(D+1)\times N(D+1)$, that contains the covariances between function values and gradients, $\boldsymbol{c}_{x_ix}$ is the same covariance vector as in (31), $\boldsymbol{F}=[1,\ldots,1,0,\ldots,0]$ (a vector with N unity values and the rest being zeros), and $\widetilde{\boldsymbol{\delta}}$ is the associated Lagrange multiplier [30]. Note that $\boldsymbol{F}$ in the GEK method can be thought of as a rudimentary version of the basis functions in UK or TK methods with the order $M=0$.

D. GRADIENT ENHANCED TAYLOR KRIGING

The use of adjoints to find gradient information has recently become more explored and exploited in computational science and engineering, so the utilization of gradients in surrogate functions is increasingly of interest. However, the gradient-enhanced Kriging method has been developed typically based on the ordinary Kriging technique. The goal here is to develop a gradient enhanced Kriging methodology based on the TK approach instead. The novel gradient-enhanced Taylor Kriging (GETK) method would then benefit from both the gradient information and the basis functions in the regression scheme. Moreover, in our approach, the gradients are obtained from the adjoint solve to the deterministic forward problem for a specific QoI.

Expanding the general Kriging predictor form in (2), we introduce a GETK predictor given by

$$\widehat{Z}(\boldsymbol{X})=\sum_{i=1}^{N}\left[\lambda_i\ Z(\boldsymbol{X}_i)\ +\ \kappa_i\frac{\partial Z(\boldsymbol{X}_i)}{\partial \boldsymbol{X}_i}\right], \tag{39}$$

thus introducing the function gradient multiplied by a second weight vector, κ. Satisfying the unbiased estimator condition, $E[Z(\boldsymbol{X})]=E[\widehat{Z}(\boldsymbol{X})]$, (7) is now expanded to

$$b_l(\boldsymbol{X})=\sum_{i=1}^{N}\left[\lambda_i b_l(\boldsymbol{X}_i)+\kappa_i\frac{\partial b_l(\boldsymbol{X}_i)}{\partial \boldsymbol{X}_i}\right],\quad l=0,1,\ldots,M. \tag{40}$$

Deriving $Var[\widehat{Z}(\boldsymbol{X}) - Z(\boldsymbol{X})]$, (3) now acquires a substantially more complex form,

$$\begin{aligned}
&\text{Minimize: } Var[\epsilon(\boldsymbol{X})] \\
&= \sum_{i=1}^{N}\lambda_i \sum_{j=1}^{N}\lambda_j Cov\big[Z(\boldsymbol{X}_i),\ Z\big(\boldsymbol{X}_j\big)\big] \\
&\quad + \sum_{i=1}^{N}\kappa_i \sum_{j=1}^{N}\lambda_j Cov\left[\frac{\partial Z(\boldsymbol{X}_i)}{\partial \boldsymbol{X}_i},\ Z\big(\boldsymbol{X}_j\big)\right] \\
&\quad + \sum_{i=1}^{N}\kappa_i \sum_{j=1}^{N}\kappa_j Cov\left[\frac{\partial Z(\boldsymbol{X}_i)}{\partial \boldsymbol{X}_i}, \frac{\partial Z\big(\boldsymbol{X}_j\big)}{\partial \boldsymbol{X}_j}\right] + Var[Z(\boldsymbol{X})] \\
&\quad + \sum_{i=1}^{N}\lambda_i \sum_{j=1}^{N}\kappa_j Cov\left[Z(\boldsymbol{X}_i), \frac{\partial Z\big(\boldsymbol{X}_j\big)}{\partial \boldsymbol{X}_j}\right] \\
&\quad - 2\sum_{i=1}^{N}\lambda_i Cov[Z(\boldsymbol{X}_i),\ Z(\boldsymbol{X})] \\
&\quad - 2\sum_{i=1}^{N}\kappa_i Cov\left[\frac{\partial Z(\boldsymbol{X}_i)}{\partial \boldsymbol{X}_i},\ Z(\boldsymbol{X})\right].
\end{aligned} \tag{41}$$

Using the same Lagrange multipliers ($\boldsymbol{\delta}$) approach and the fact that

$$Cov\left[\frac{\partial Z(\boldsymbol{X}_i)}{\partial \boldsymbol{X}_i},\ Z\big(\boldsymbol{X}_j\big)\right] = \frac{\partial}{\partial \boldsymbol{X}_i} Cov\big[Z(\boldsymbol{X}_i),\ Z\big(\boldsymbol{X}_j\big)\big], \tag{42}$$

the system in (41) can be recast as

$$\begin{bmatrix}\boldsymbol{\lambda}\\ \boldsymbol{\kappa}\\ \boldsymbol{\delta}\end{bmatrix} = \begin{bmatrix} \boldsymbol{C} & \frac{\partial \boldsymbol{C}}{\partial \boldsymbol{X}_j} & \boldsymbol{B} \\ \frac{\partial \boldsymbol{C}^T}{\partial \boldsymbol{X}_i} & \frac{\partial^2 \boldsymbol{C}}{\partial \boldsymbol{X}_i \partial \boldsymbol{X}_j} & \frac{\partial \boldsymbol{B}}{\partial \boldsymbol{X}_i} \\ \boldsymbol{B}^T & \frac{\partial \boldsymbol{B}^T}{\partial \boldsymbol{X}_i} & \boldsymbol{0} \end{bmatrix}^{-1} \begin{bmatrix} \boldsymbol{c}_{x_i x} \\ \frac{\partial c_{x_i x}}{\partial x_i} \\ \boldsymbol{b}_{\boldsymbol{X}} \end{bmatrix}. \tag{43}$$

The so obtained GETK matrix system can then be solved for weights $\boldsymbol{\lambda}$ and $\boldsymbol{\kappa}$, which constitute the solution for the GETK predictor $\widehat{Z}(\boldsymbol{X})$ in (39).

The GETK system main matrix can be formally interpreted as the GEK one in (38) with $\dot{\boldsymbol{C}}$ and $\boldsymbol{F}$ now containing covariances and basis functions, respectively, as well as their derivatives,

$$\dot{\boldsymbol{C}} = \begin{bmatrix} \boldsymbol{C} & \frac{\partial \boldsymbol{C}}{\partial \boldsymbol{X}_i} \\ \frac{\partial \boldsymbol{C}}{\partial \boldsymbol{X}_j} & \frac{\partial^2 \boldsymbol{C}}{\partial \boldsymbol{X}_i \partial \boldsymbol{X}_j} \end{bmatrix},\ \boldsymbol{F} = \begin{bmatrix} \boldsymbol{B} \\ \frac{\partial \boldsymbol{B}}{\partial \boldsymbol{X}_i} \end{bmatrix}. \tag{44}$$

Note, however, that the largest computational load in performing both GEK and GETK methods comes from inverting the composite covariance matrix, $\dot{\boldsymbol{C}}$, which is the same size for both methods. This means that there is very little extra computational cost for using GETK as compared to GEK.

The MLE formulation for covariance function, described in Section II-C, has an additional benefit when used within the GEK and GETK methods, where the gradients are considered. Since we have an explicit form for the covariance function as opposed to a fitted function in the case of the empirical covariance, we can explicitly evaluate covariance function derivatives. The derivatives in (43), which are Jacobians in general dimension, are calculated using the form of covariance in (14) and (15) as follows:

$$\frac{\partial \boldsymbol{C}}{\partial \boldsymbol{X}_i} = \Big[-2\theta^{(k)}\Big(X_{\boldsymbol{i}}^{(\boldsymbol{k})} - X_{\boldsymbol{j}}^{(\boldsymbol{k})}\Big)\sigma^2 R\big(\boldsymbol{X}_i,\ \boldsymbol{X}_j,\ \theta\big)\Big]_{k=1,\ldots,D} \tag{45}$$

$$\frac{\partial \boldsymbol{C}}{\partial \boldsymbol{X}_j} = \Big[2\theta\Big(X_{\boldsymbol{i}}^{(\boldsymbol{k})} - X_{\boldsymbol{j}}^{(\boldsymbol{k})}\Big)\sigma^2 R\big(\boldsymbol{X}_i,\ \boldsymbol{X}_j,\ \theta\big)\Big]_{k=1,\ldots,D} \tag{46}$$

$$\begin{aligned}
&\frac{\partial^2 \boldsymbol{C}}{\partial \boldsymbol{X}_i \partial \boldsymbol{X}_j} \\
&= \begin{cases} \left[\begin{pmatrix} 2\theta X_{\boldsymbol{i}}^{(\boldsymbol{k})^2} - 4\theta X_i^{(k)} X_j^{(k)} \\ +2\theta X_j^{(k)^2} - 1 \end{pmatrix} \cdot -2\theta^{(k)}\sigma^2 R\big(\boldsymbol{X}_i,\ \boldsymbol{X}_j,\ \theta\big)\right]_{k,l=1,\ldots,D} & \text{for } k = l \\ \left[\begin{matrix} -4\theta^{(k)}\theta^{(l)} \\ \cdot\Big(X_i^{(k)} - X_j^{(k)}\Big) \\ \cdot\Big(X_i^{(l)} - X_j^{(l)}\Big)\sigma^2 R\big(\boldsymbol{X}_i,\ \boldsymbol{X}_j,\ \theta\big) \end{matrix}\right]_{k,l=1,\ldots,D} & \text{otherwise} \end{cases}
\end{aligned} \tag{47}$$

where the sizes of these Jacobian terms are $N \times ND$ for (45) and (46) and $ND \times ND$ for (47). On the other hand, when using the empirical covariance method, the derivatives must be computed numerically using finite differences or similar techniques. Additionally, matrix conditioning can be a concern in many regression and interpolation schemes, and to counter this issue in the Kriging methods, a small term is added to the diagonal of the composite covariance matrix, $\dot{\boldsymbol{C}}$, which helps with numerical stability of the output.

It is interesting to note that the Kriging model itself is inherently a stochastic model. So, while we propagate uncertainty from a stochastic input variable to the output, the model itself adds to the overall uncertainty, compared with the Monte Carlo solution which is deterministic. A full coverage of this can be found in [42], where we see that the first moment of uncertainty, i.e., the mean, is unaffected, whereas the variance of UQ is biased by the stochasticity of the model. Additionally, this additional uncertainty due to the model becomes very small as the number of samples increases, and the study of the exact uncertainty of the model and its effect on the overall uncertainty of the problem becomes intractable as input parameter dimension becomes large.

IV. RESULTS AND DISCUSSION

We now present numerical results obtained in comparison of five different Kriging approaches, namely, OK, UK, TK, GEK, and GETK methods, as well as two well-established non-Kriging UQ methodologies, the HOPS adjoint sensitivity analysis method [2], [3] and the PCE method implemented as an aPC technique [50], [56], in UQ scattering problems. The performance of each of the presented methods and solutions is assessed in comparison with the 1000-point Monte Carlo

(MC) simulation as a reference solution and a validation norm.

The scattering analysis is done using higher order curvilinear FEM modeling [57], [58], [59] to solve the double-curl wave equation (19) for the scattered field $\boldsymbol{E}^{sc}$ with an anisotropic locally-conformal perfectly matched layer (PML) for the computational domain termination [60]. The QoI considered here is the monostatic radar cross section (RCS) of a lossy dielectric sphere, with a goal of predicting material uncertainty impact on FEM-PML RCS computations.

In all of the Kriging results in this work, we use MLE to construct the covariance function (Section II-C) as an alternative to the empirical covariance function (Section II-B). In UK, TK, and GETK implementations and simulations, we adopt the number of basis functions, M, according to the maximum limit allowed by (35) given the dimension of the parameter space, D, and the adopted number of input sample points, N, in particular test cases and analyses. In addition, we separately limit the bases to a maximum of $M = 5$, to avoid ringing effects from high degree polynomial basis functions, also known as Runge phenomenon [61]. The OK and GEK implementations are inherently limited to 0^{th} order bases ($M = 0$).

In all cases tested here, we use a uniform sampling distribution of (N) input sample (training) points. While individual Kriging implementations frequently construct an initial discretization using Latin hypercube sampling (LHS) or similar method and then adaptively and optimally refine the distribution of points using a variety of techniques such as adaptive sampling, an even distribution of sample points where each method performs reconstruction using the same set of points was deemed to be the most appropriate for comparative numerical studies and evaluation of different techniques in this work. Here, even sampling becomes intractable in higher dimensions since the parameter space volume grows exponentially with the dimension increase. Instead, LHS or similar sampling schemes are typically chosen for the initial data set. This also means that to sample the input space with the same density with an increase in dimension, N must increase exponentially as well. Additionally, the size of the Kriging system matrix, whose inversion represents the bulk of the computational load for the model, grows as $N(D+1) \times N(D+1)$, which can also become quite large as both N and D increase. This is known as the curse of dimensionality, mentioned earlier, a well-known phenomenon with many models involving sampling, including aPC and Kriging. The mitigation of these effects is a well-researched problem, which, however, is outside of the scope of this work.

We also note that the initial set of sampled training data can have a significant effect on the predicted value from the trained Kriging model. In some cases, where sampling does not adequately sample the parameter space, the initial predicted value can have poor performance. By either increasing the number of samples or changing the initial sample distribution, we can dramatically increase the accuracy of the initial Kriging prediction. LHS is a model that generates random test points that fully sample the input parameter space, and is thus typically used to sample parameter space in high dimension. In this work, we avoid using such sampling in order to keep an even distribution so that all comparisons of different methods are done on equal base.

In all cases, the input variable is assumed to be a random variable, and we sample 1000 points to form the input distribution. For the Monte Carlo reference simulation, we compute the solution at each of the 1000 sample points using higher order FEM modeling, which forms the deterministic solution; however, this can very quickly become intractable with computationally heavy simulations. The same sampled input distribution is then used to predict the RCS and the probability density function using the trained Kriging model, where we evaluate the error with respect to the MC method as our metric.

A. TEST CASE WITH SMOOTH OUTPUT FUNCTION

As our first test case, we consider the scattered field of a spherical dielectric scatterer 2 m in diameter excited by a plane electromagnetic wave at 70 MHz. The scatterer material property constitutes the uncertain input parameter, with the real part of the relative permittivity, ε_r, described by a normal random variable (the dimension of the parameter space is $D = 1$). The complex relative permittivity is given by $\varepsilon_r = \{\sim N(6, 1.5), -2\}$, where the real part of ε_r is described as a normal random distribution with mean equal to 6 and variance 1.5 and the imaginary part is taken to be constant with a value of -2. We establish the validity and examine the performance of each of the presented methods in comparison with a reference 1000-point Monte Carlo simulation, treated as an "exact" solution.

In Fig. 1, we examine the convergence of the root mean squared error (RMSE) of the surrogate reconstruction of the probability density function versus the number of input sample points by means of the five presented Kriging methods, as well as HOPS and PCE methods, with respect to the reference Monte Carlo simulation. We observe relatively good convergence for many methods, coming from the fact that a well-behaved, smooth, output function is relatively easy to predict using different methods. However, even with this well-behaved result, we still see that the novel GETK method outperforms all other approaches by orders of magnitude. In addition, note that the HOPS method is used, along with the PCE method, as a non-Kriging comparison case for these results, but it should be emphasized that while this excellent UQ approach might require a larger number of sample points to achieve accurate results, with large input vectors, its true strength lies in the ability to accurately and efficiently predict UQ problems with higher dimensions of parameter spaces [2], [3].

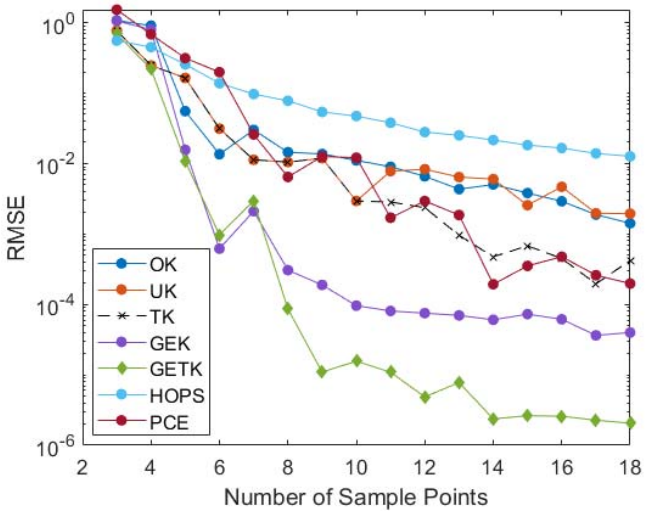

FIGURE 1. Convergence of the root mean squared error of the RCS surrogate reconstruction of a dielectric spherical scatterer 2 m in diameter, with uncertain relative permittivity given by a normal random distribution $\varepsilon_r = \{\sim N(6, 1.5), -2\}$, excited by a plane wave at 70 MHz: comparison of results obtained by five different Kriging methods, HOPS, and PCE, with RMSE computed with respect to the reference 1000-point Monte Carlo simulation considered as an "exact" solution.

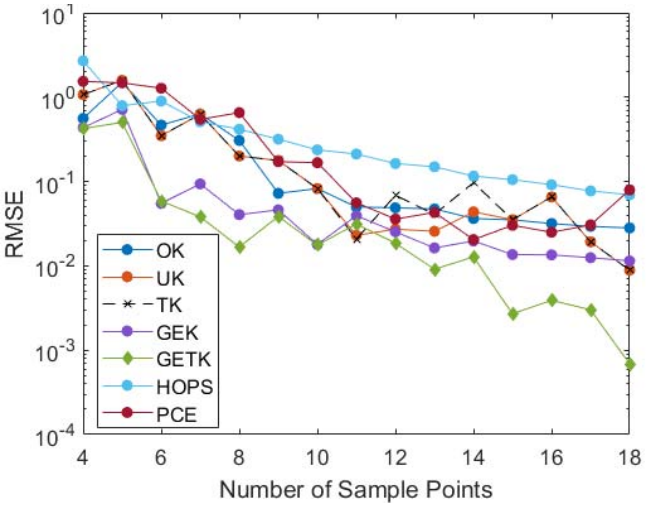

FIGURE 2. RCS reconstruction RMSE convergence for the five Kriging methods, HOPS, and PCE for a 2-m diameter spherical dielectric scatterer with input uncertain relative permittivity given by $\varepsilon_r = \{\sim N(6, 1.5), -1\}$ at 115 MHz. taking the reference 1000-point Monte Carlo results as an "exact" solution.

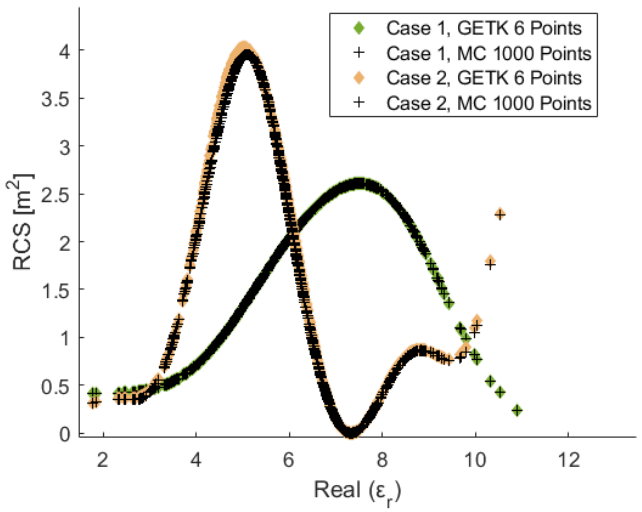

FIGURE 3. Comparison of output RCS surrogate reconstructions obtained by the novel GETK method, at 6 reconstruction points, with the reference 1000-point Monte Carlo (MC) simulations for the dielectric spherical scatterer analyzed in Fig. 1 (case 1) and that from Fig. 2 (case 2).

B. TEST CASE WITH RAPIDLY VARYING OUTPUT FUNCTION

Our second test case deals with the RCS of a 2-m diameter spherical dielectric scatterer with $D = 1$ and $\varepsilon_r = \{\sim N(6, 1.5), -1\}$ at 115 MHz. The goal of this second comparative study is to examine the convergence of different Kriging methods with a rapidly varying output solution, as this represents a difficult case for any data reconstruction method. The RMSE probability density function reconstruction results in Fig. 2 demonstrate that the GETK method indeed converges much faster than all other techniques tested. We see that the GEK method performs quite well also, but still considerably underperforms the GETK results. Overall, for each of the presented methods, we observe much higher accuracy in Fig. 1, in the well-behaved output function case, than in Fig. 2 for the same number of sample points. Namely, in this case we see just how difficult it is to use a surrogate model when the output gradients vary significantly. Finally, a study like the one in Fig. 2 indeed gives a quantitative measure of how much more accurate a UQ method (the GETK method here) is in reconstructing the uncertainty of CEM problems, that is, in outputting probability density prediction for a quantity of interest given the probability density of an uncertain (stochastic) input parameter.

With the previously presented convergence studies having established the novel GETK method as clearly the best performing choice, Fig. 3 shows the GETK reconstruction of the RCS QoI given only 6 sample points, for both the smoothly and rapidly varying test cases of Figs. 1 and 2, respectively. We see an almost exact agreement between GETK surrogate function results, at an extremely small number of sample points, and the reference 1000-point Monte Carlo solution, which demonstrates excellent reconstruction capability of the GETK method. Whereas the error convergence studies (in Figs. 1 and 2) are by all means most relevant for validation and comparative evaluation of different numerical approaches and techniques, the explicit results for the probability density function reconstruction as a function of the RCS QoI shown in Fig. 4 are perhaps the most practically important, as the principal goal of a UQ method is to reproduce an output probability density that most closely matches the true value. These results show that the probability density reconstruction by means of the novel GETK method is extremely accurate even with as few as 6 sample points in both test cases, when compared to the reference 1000-point Monte Carlo solution.

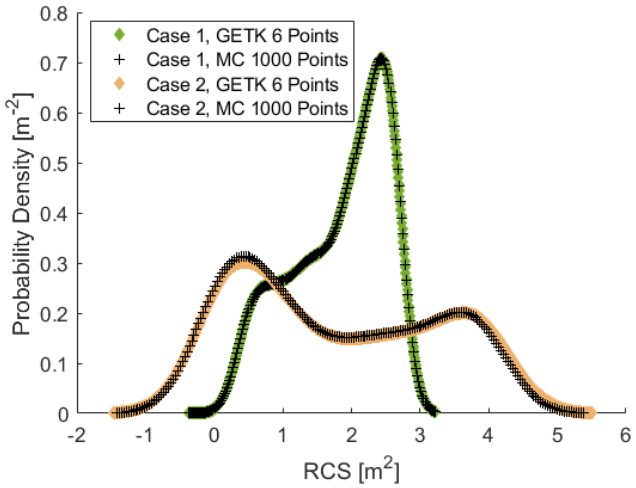

FIGURE 4. Predicted output probability density function for the RCS QoI of two dielectric spherical scatterers (cases 1 and 2) analyzed in Fig. 3: comparison of results obtained by the novel GETK method at 6 reconstruction points with the reference 1000-point Monte Carlo simulations.

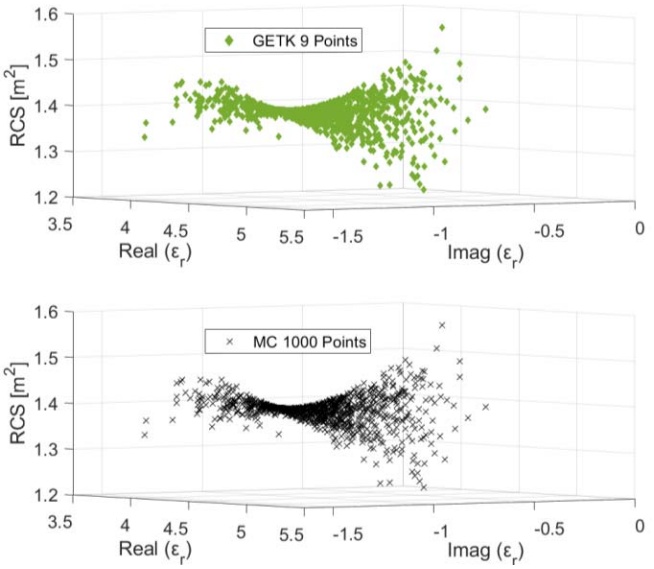

FIGURE 5. Comparison of the output RCS GETK surrogate reconstruction, at 9 reconstruction points, with the 1000-point Monte Carlo results for a 2-m diameter spherical dielectric scatterer with both the real and imaginary components of the permittivity independently undergoing random variations, $\varepsilon_r = \{\sim N(4.5,\ 0.25),\ \sim N(-1, 0.25)\}$, at 50 MHz.

C. TEST CASE WITH MULTI-PARAMETER UNCERTAINTY

Our third test case deals with multi-parameter or higher-dimensional uncertainty, namely, with a problem where more than one input parameter in the model undergoes random variation. As this work compares and discusses different Kriging (and non-Kriging) solutions to UQ scattering problems and examines the accuracy and convergence of the solution and performance of various approaches with emphasis on predicting material uncertainty impact on FEM RCS computations, the most natural multi-parameter uncertainty and higher-dimensional input in this context seems to be a 2-dimensional ($D = 2$) perturbation of both the real and imaginary components of the dielectric permittivity of the scatterer. Hence, we consider the RCS of a 2-m diameter spherical dielectric scatterer with both the real and imaginary parts of ε_r being described independently by a normal random variable, $\varepsilon_r = \{\sim N(4.5, 0.25), \sim N(-1, 0.25)\}$, at 50 MHz, to verify the accuracy of the presented UQ approaches and examine the convergence of different Kriging methods. The output Monte Carlo RCS reconstruction for this test case is the classical "saddle" shape, shown in Fig. 5, which represents an excellent test case for many numerical methods due to an unstable critical point that acts as both a local minimum and maximum depending on the axis. This test case should be challenging for surrogate functions due to both the higher dimensionality of the input as well as the output shape.

Fig. 5 also shows the RCS reconstruction of the surrogate function using the novel GETK method with only 9 sample points, where we observe a perfect match with the reference 1000-point Monte Carlo simulation. In fact, the agreement is so close that the 3-D rendering for this figure when the two sets of results are shown on top of each other would have a difficult time distinguishing between the two "saddle" surfaces. Hence, the results in Fig. 5 are presented in two separate figures, to better show the two data sets while still demonstrating how similar/exact they are when compared to each other and how the GETK RCS reconstruction is almost an exact match with MC solution even with an extremely small number of training input points.

Inspecting the convergence of the RMSE of the probability density function reconstruction versus the number of sample points using the five Kriging methods, HOPS, and PCE in Fig. 6, we conclude that the novel GETK method indeed converges much faster than all other techniques tested. We also see that the PCE method, which is considered to be an excellent surrogate model for UQ, starts to perform quite well at large numbers of sample points; however, a much more rapid convergence and lower error of GEK and especially GETK methods with lower numbers of points are observed.

Fig. 7 shows the probability density distribution of the 2-D random case predicted using GETK from 9 sample points compared with the 1000-point Monte Carlo simulation. We observe that the novel GETK method matches the reference solution remarkably well and predicts a practically "exact" output density function for the RCS QoI with an extremely small number of points. Additionally, the figure includes for reference the results for the 1-D random case in which the input probability density has been collapsed to the mean in the imaginary part of ε_r. This demonstrates the importance of modeling all uncertain input variables in the model, as the addition of a second randomly varied parameter significantly affects the output probability density function for the considered quantity of interest.

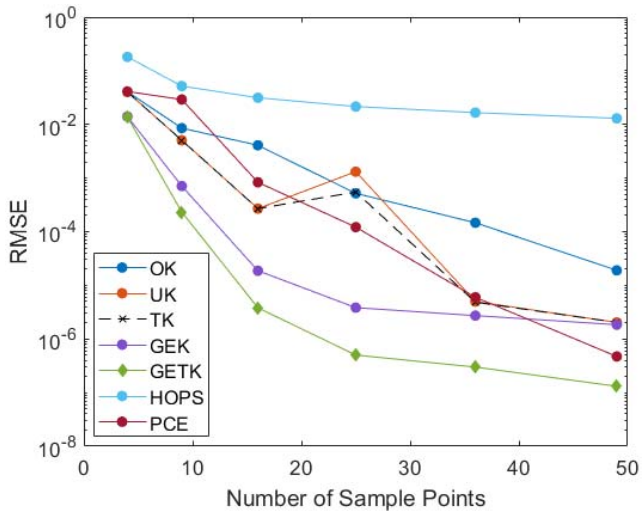

FIGURE 6. Convergence of the RMSE of the probability density function reconstruction versus the number of sample points using the five Kriging methods, HOPS, and PCE for the dielectric spherical scatterer with 2-D uncertainty analyzed in Fig. 5, with the 1000-point Monte Carlo simulation as a validation norm.

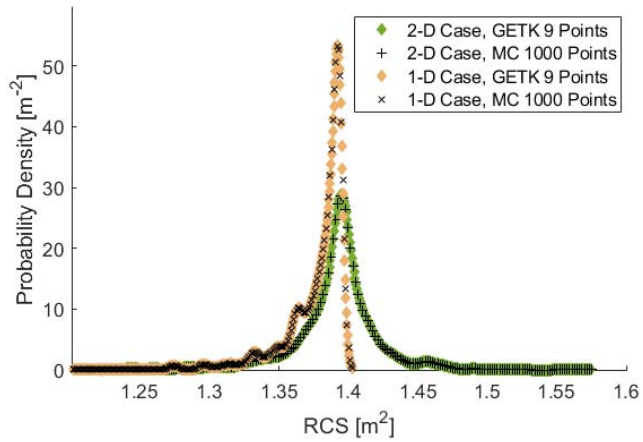

FIGURE 7. Comparison of the probability density reconstruction as a function of RCS QoI for the dielectric spherical scatterer with the 2-D parameter space from Fig. 5 generated by the novel GETK method at 9 reconstruction points with the reference 1000-point Monte Carlo solution. Overlayed are also the results for the 1-D random case with the probability density of the imaginary part of ε_r collapsed to its mean, $\varepsilon_r = \{\sim N(4.5, 0.25), -1\}$.

V. CONCLUSION

This paper has presented the implementation and use of the Kriging methodology in uncertainty quantification in computational electromagnetics. It has provided consistent and unified description, derivation, implementation, and use of several advanced Kriging approaches, namely, the universal Kriging, Taylor Kriging, and gradient-enhanced Kriging methods, for reconstruction of probability density function in CEM problems. The paper has offered in-depth and comprehensive description of Kriging, as well as the necessary methods to calculate covariance, adjoints, correlation, etc., so that interested readers could use this material to construct their own Kriging method with little to no extra resources needed.

The paper has also proposed, derived, and demonstrated the gradient-enhanced Taylor Kriging methodology, novel to science and engineering in general. The novel GETK approach combines the advantages of all other methods. It benefits from both the gradient information, like with the GEK method, and basis functions in the regression scheme, as in the UK and TK formulations. Moreover, in our approach, the gradients are calculated from the suitable adjoint problem that relates the deterministic forward problem to a specific quantity of interest. This is the first application of gradient enhanced Kriging with basis functions to CEM problems.

The paper has presented validation and comparative numerical studies of five different Kriging solutions to UQ scattering problems and has examined the accuracy and convergence of the solution and performance of various approaches. Numerical results using higher order curvilinear FEM-PML scattering modeling have shown that the presented Kriging methods are able to accurately and efficiently output probability density prediction for a quantity of interest (RCS of a scatterer) given the probability density of stochastic input parameters (material uncertainties), with very small numbers of sample (training) points, as a very efficient alternative to Monte Carlo simulations.

The novel GETK method has vastly outperformed all other approaches, Kriging (OK, UK, TK, and GEK) and non-Kriging (HOPS and PCE), in terms of surrogate function accuracy and convergence with increasing the number of sample points in all examples. While this work has shown Kriging and other results for 1-dimensional and 2-dimensional uncertainties that seemed to be the most natural inputs in the context of predicting material uncertainty impact on FEM RCS computations, the demonstrated advancement of the accuracy with the novel GETK method over all other approaches should translate to higher dimensional surrogate problems as well and is not limited to lower dimensional inputs.

REFERENCES

[1] R. Smith, *Uncertainty Quantification: Theory, Implementation, and Applications*. Philadelphia, PA, USA: SIAM, 2014.
[2] J. J. Harmon, C. Key, D. Estep, T. Butler, and B. M. Notaroš, "Adjoint sensitivity analysis for uncertain material parameters in frequency domain 3-D FEM," *IEEE Trans. Antennas Propag.*, vol. 69, no. 10, pp. 6669–6679, Oct. 2021.
[3] J. J. Harmon and B. M. Notaros, "Reducing the computational expense of uncertainty quantification in computational electromagnetics: A goal-oriented perspective," in *Proc. IEEE Int. Symp. Antennas Propag.*, 2022, pp. 659–660.
[4] D. Estep and D. Neckels, "Fast methods for determining the evolution of uncertain parameters in differential equations," *J. Comput. Phys.*, vol. 213, no. 2, pp. 530–556, Apr. 2006.
[5] D. Estep and D. Neckels, "Fast methods for determining the evolution of uncertain parameters in reaction-diffusion equations," *Comput. Methods Appl. Mech. Eng.*, vol. 196, pp. 3967–3979, Aug. 2007.
[6] J. H. S. Baar, "Stochastic surrogates for measurements and computer models of fluids," Ph.D. Dissertaition, Dept. Aerodynamics, Delft Univ. Technol., Delft, The Netherlands, Dec. 2014.
[7] R. L. Wagner, J. Song, and W. C. Chew, "Monte Carlo simulation of electromagnetic scattering from two-dimensional random rough surfaces," *IEEE Trans. Antennas Propag.*, vol. 45, no. 2, pp. 235–245, Feb. 1997.

[8] Q. Li, H. Chan, and L. Tsang, "Monte Carlo simulations of wave scattering from lossy dielectric random rough surfaces using the physics-based two-grid method and the canonical-grid method," *IEEE Trans. Antennas Propag.*, vol. 47, no. 4, pp. 752–763, Apr. 1999.

[9] N. Garcia and E. Stoll, "Monte Carlo calculation for electromagnetic wave scattering from random rough surfaces," *Phys. Rev. Lett.*, vol. 52, pp. 1798–1801, May 1984.

[10] S. M. Smith and C. Furse, "Stochastic FDTD for analysis of statistical variation in electromagnetic fields," *IEEE Trans. Antennas Propag.*, vol. 60, no. 7, pp. 3343–3350, Jul. 2012.

[11] K. Masumnia-Bisheh, K. Forooraghi, and M. Ghaffari-Miab, "Electromagnetic uncertainty analysis using stochastic FDFD method," *IEEE Trans. Antennas Propag.*, vol. 67, no. 5, pp. 3268–3277, May 2019.

[12] A. C. M. Austin and C. D. Sarris, "Efficient analysis of geometrical uncertainty in the FDTD method using polynomial chaos with application to microwave circuits," *IEEE Trans. Microw. Theory Techn.*, vol. 61, no. 12, pp. 4293–4301, Dec. 2013.

[13] R. S. Edwards, A. C. Marvin, and S. J. Porter, "Uncertainty analyses in the finite-difference time-domain method," *IEEE Trans. Electromagn. Compat.*, vol. 52, no. 1, pp. 155–163, Feb. 2010.

[14] U. K. Khankhoje and S. Padhy, "Stochastic solutions to rough surface scattering using the finite element method," *IEEE Trans. Antennas Propag.*, vol. 65, no. 8, pp. 4170–4180, Aug. 2017.

[15] G. J. K. Tomy and K. J. Vinoy, "A fast polynomial chaos expansion for uncertainty quantification in stochastic electromagnetic problems," *IEEE Antennas Wireless Propag. Lett.*, vol. 18, no. 10, pp. 2120–2124, Oct. 2019.

[16] G. J. K. Tomy and K. J. Vinoy, "Neumann-expansion-based FEM for uncertainty quantification of permittivity variations," *IEEE Antennas Wireless Propag. Lett.*, vol. 19, no. 4, pp. 561–565, Apr. 2020.

[17] M. Branicki and A. Majda, "Fundamental limitations of polynomial chaos for uncertainty quantification in systems with intermittent instabilities," *Commun. Math. Sci.*, vol. 11, no. 1, pp. 55–103, 2013.

[18] D. Voyer, F. Musy, L. Nicolas, and R. Perrussel, "Comparison of methods for modeling uncertainties in a 2D hyperthermia problem," *Progr. Electromagn. Res. B*, vol. 11, pp. 189–204, Jan. 2009.

[19] M. A. Drissaoui et al., "A stochastic collocation method combined with a reduced basis method to compute uncertainties in numerical dosimetry," *IEEE Trans. Magn.*, vol. 48, no. 2, pp. 563–566, Feb. 2012.

[20] J. Ochoa and A. Cangellaris, "Macro-modeling of electromagnetic domains exhibiting geometric and material uncertainty," *Appl. Comput. Electromagn. Soc. J.*, vol. 27, no. 2, pp. 80–87, 2012.

[21] M. Gossye, G. Gordebeke, K. Y. Kapusuz, D. V. Ginste, and H. Rogier, "Uncertainty quantification of waveguide dispersion using sparse grid stochastic testing," *IEEE Trans. Microw. Theory Techn.*, vol. 68, no. 7, pp. 2485–2494, Jul. 2020.

[22] D. Poljak, S. Šesnić, M. Cvetković, S. Lallechere, and K. El Khamlichi Drissi, "On some applications of stochastic collocation method in computational electromagnetics: Applications in ground penetrating radar, bioelectromagnetics, grounding systems and buried lines," in *Proc. 24th Int. Conf. Softw. Telecommun. Comput. Netw. (SoftCOM)*, 2016, pp. 1–5.

[23] J. Son and Y. Du, "Comparison of intrusive and nonintrusive polynomial chaos expansion-based approaches for high dimensional parametric uncertainty quantification and propagation," *Comput. Chem. Eng.*, vol. 134, Mar. 2020, Art. no. 106685.

[24] M. Eldred, "Recent advances in non-intrusive polynomial chaos and stochastic collocation methods for uncertainty analysis and design," in *Proc. 50th AIAA/ASME/ASCE/AHS/ASC Struct., Struct. Dyn., Mater. Conf.*, 2009, pp. 1–37.

[25] Y. Li, G. Lei, G. Bramerdorfer, S. Peng, X. Sun, and J. Zhu, "Machine learning for design optimization of electromagnetic devices: recent developments and future directions," *Appl. Sci.*, vol. 11, no. 4, p. 1627, 2021.

[26] M. O. Akinsolu, K. K. Mistry, B. Liu, P. I. Lazaridis, and P. Excell, "Machine learning-assisted antenna design optimization: A review and the state-of-the-art," in *Proc. 14th Eur. Conf. Antennas Propag. (EuCAP)*, 2020, pp. 1–5.

[27] Q. Wu, H. Wang, and W. Hong, "Multistage collaborative machine learning and its application to antenna modeling and optimization," *IEEE Trans. Antennas Propag.*, vol. 68, no. 5, pp. 3397–3409, May 2020.

[28] D. Kan, D. Spina, S. De Ridder, F. Grassi, H. Rogier, and D. V. Ginste, "A machine-learning-based epistemic modeling framework for textile antenna design," *IEEE Antennas Wireless Propag. Lett.*, vol. 18, no. 11, pp. 2292–2296, Nov. 2019.

[29] R. P. Dwight and Z.-H. Han, "Efficient uncertainty quantification using gradient-enhanced Kriging," in *Proc. 11th AIAA Non-Deterministic Approaches Conf.*, 2009, pp. 1–23.

[30] W. Yamazaki, M. P. Rumpfkeil and D. J. Mavriplis, "Design optimization utilizing gradient/Hessian enhanced surrogate model," in *Proc. 28th AIAA Appl. Aerodyn. Conf.*, Chicago, IL, USA, Jun./Jul. 2010, pp. 1–23.

[31] J. Peter and M. Marcelet, "Comparison of surrogate models for turbomachinery design," *WSEAS Trans. Fluid Mech.*, vol. 3, no. 1, pp. 10–17, Jan. 2008.

[32] H.-S. Chung and J. J. Alonso, "Using gradients to construct coKriging approximation models for high-dimensional design optimization problems," in *Proc. 40th AIAA Aerosp. Sci. Meeting Exhibit*, Reno, NV, USA, Jan. 2002, pp. 1–15.

[33] L. Zhao, K. K. Choi, and I. Lee, "Metamodeling method using dynamic Kriging for design optimization," *AIAA J.*, vol. 49, no. 9, pp. 2034–2046, Sep. 2011.

[34] S. Bhattacharjee, P. Mitra, and S. K. Ghosh, "Spatial interpolation to predict missing attributes in GIS using semantic Kriging," *IEEE Trans. Geosci. Remote Sens.*, vol. 52, no. 8, pp. 4771–4780, Aug. 2014.

[35] S. Yu and Y. Li, "Active learning Kriging model with adaptive uniform design for time-dependent reliability analysis," *IEEE Access*, vol. 9, pp. 91625–91634, 2021.

[36] B. Xia, T. Lee, K. Choi, and C. Koh, "A novel adaptive dynamic Taylor Kriging and its application to optimal design of electromagnetic devices," *IEEE Trans. Magn.*, vol. 52, no. 3, pp. 1–4, Mar. 2016.

[37] E. S. Siah, M. Sasena, J. L. Volakis, P. Y. Papalambros, and R. W. Wiese, "Fast parameter optimization of large-scale electromagnetic objects using DIRECT with Kriging metamodeling," *IEEE Trans. Microw. Theory Techn.*, vol. 52, no. 1, pp. 276–285, Jan. 2004.

[38] A. Pietrenko-Dabrowska, S. Koziel, and M. Al-Hasan, "Accurate modeling of antenna structures by means of domain confinement and gradient-enhanced Kriging," in *Proc. 15th Eur. Conf. Antennas Propag. (EuCAP)*, Dusseldorf, Germany, 2021, pp. 1–5.

[39] A. Pietrenko-Dabrowska and S. Koziel, "Antenna modeling using variable-fidelity em simulations and constrained co-Kriging," *IEEE Access*, vol. 8, pp. 91048–91056, 2020.

[40] S. Koziel and S. Ogurtsov, "Multi-objective design of antennas using variable-fidelity simulations and surrogate models," *IEEE Trans. Antennas Propag.*, vol. 61, no. 12, pp. 5931–5939, Dec. 2013.

[41] A. Pietrenko-Dabrowska, S. Koziel, and M. Al-Hasan, "Cost-efficient bi-layer modeling of antenna input characteristics using gradient Kriging surrogates," *IEEE Access*, vol. 8, pp. 140831–140839, 2020.

[42] P. Manfredi and R. Trinchero, "A probabilistic machine learning approach for the uncertainty quantification of electronic circuits based on gaussian process regression," *IEEE Trans. Comput.-Aided Design Integr. Circuits Syst.*, vol. 41, no. 8, pp. 2638–2651, Aug. 2022.

[43] P. Manfredi, "Probabilistic uncertainty quantification of microwave circuits using gaussian processes," *IEEE Trans. Microw. Theory Techn.*, vol. 71, no. 6, pp. 2360–2372, Jun. 2023.

[44] S. Kasdorf, J. Harmon, and B. M. Notaros, "Kriging methodology for predicting material uncertainty impact on FEM scattering computations," in *Proc. IEEE Int. Symp. Antennas Propag.*, Portland, Oregon, Jul. 2023, pp. 53–54.

[45] S. Ulaganathan, I. Couckuyt, T. Dhaene, E. Laermans, and J. Degroote, "On the use of gradients in Kriging surrogate models," in *Proc. Winter Simulat. Conf.*, Savannah, GA, USA, 2014, pp. 2692–2701.

[46] C. Key, A. Smull, D. Estep, T. Butler, and B. M. Notaros, "A posteriori error estimation and adaptive discretization refinement using adjoint methods in CEM: A study with a one-dimensional higher-Order FEM scattering example," *IEEE Trans. Antennas Propag.*, vol. 68, no. 5, pp. 3791–3806, May 2020.

[47] J. J. Harmon, C. Key, D. Estep, T. Butler, and B. M. Notaros, "Adjoint-based accelerated adaptive refinement in frequency domain 3-D finite element method scattering problems," *IEEE Trans. Antennas Propag.*, vol. 69, no. 2, pp. 940–949, Feb. 2021.

[48] C. Key, J. J. Harmon, and B. M. Notaros, "Correlations in a posteriori error trends for the finite element method in the presence of changing material parameters," *IEEE Antennas Wireless Propag. Lett.*, vol. 20, no. 12, pp. 2516–2518, Dec. 2021.

[49] J. J. Harmon and B. M. Notaroš, "Accelerated adaptive error control and refinement for SIE scattering problems," *IEEE Trans. Antennas Propag.*, vol. 70, no. 10, pp. 9497–9510, Oct. 2022.
[50] S. Oladyshkin and W. Nowak, "Data-driven uncertainty quantification using the arbitrary polynomial chaos expansion," *Rel. Eng. Syst. Safety*, vol. 106, pp. 179–190, Oct. 2012.
[51] H. Liu, "Taylor Kriging metamodeling for simulation interpolation, sensitivity analysis, and optimization," Ph.D. dissertation, Dept. Ind. Syst. Eng., Univ. Auburn, Auburn, AL, USA, May 2009.
[52] M. Diago-Mosquera, A. Aragon-Zavala, L. Azpilicueta, R. Shubair, and F. Falcone, "A 3-D indoor analysis of path loss modeling using Kriging techniques," *IEEE Antennas Wireless Propag. Lett.*, vol. 21, no. 6, pp. 1218–1222, Jun. 2022.
[53] P. Wang, Z. Feng, Y. Tang, and Y. Zhang, "A fingerprint database reconstruction method based on ordinary Kriging algorithm for indoor localization," in *Proc. Int. Conf. Intell. Transport. Big Data Smart City*, 2019, pp. 224–227.
[54] G. I. Marchuk, *Adjoint Equations and Analysis of Complex Systems*. Dordrecht, The Netherlands: Kluwer Acad. Publ., 1995.
[55] B. Xia, N. Baatar, Z. Ren, and C.-S. Koh, "A numerically efficient multi-objective optimization algorithm: Combination of dynamic Taylor Kriging and differential evolution," *IEEE Trans. Magn.*, vol. 51, no. 3, pp. 1–4, Mar. 2015.
[56] S. Oladyshkin. "aPC Matlab toolbox: Data-driven arbitrary polynomial chaos." MATLAB Central File Exchange. Jul. 5, 2023. [Online]. Available: https://www.mathworks.com/matlabcentral/fileexchange/72014-apc-matlab-toolbox-data-driven-arbitrary-polynomial-chaos
[57] M. M. Ilic and B. M. Notaros, "Higher order hierarchical curved hexahedral vector finite elements for electromagnetic modeling," *IEEE Trans. Microw. Theory Techn.*, vol. 51, no. 3, pp. 1026–1033, Mar. 2003.
[58] M. M. Ilic and B. M. Notaros, "Higher order large-domain hierarchical FEM technique for electromagnetic modeling using Legendre basis functions on generalized hexahedra," *Electromagnetics*, vol. 26, no. 7, pp. 517–529, 2006.
[59] B. M. Notaros, "Higher order frequency-domain computational electromagnetics," *IEEE Trans. Antennas Propag.*, vol. 56, no. 8, pp. 2251–2276, Aug. 2008.
[60] A. P. Smull, A. B. Manic, S. B. Manic, and B. M. Notaros, "Anisotropic locally-conformal perfectly matched layer for higher order curvilinear finite-element modeling," *IEEE Trans. Antennas Propag.*, vol. 65, no. 12, pp. 7157–7165, Dec. 2017.
[61] J. Epperson, "On the Runge example," *Amer. Math. Month.*, vol. 94, no. 4, pp. 329–341, 1987.

STEPHEN KASDORF (Student Member, IEEE) received the B.S. degree (magna cum laude) in electrical engineering and applied physics from Colorado State University in 2019, where he is currently pursuing the Ph.D. degree in electrical engineering.

His research interests include high frequency asymptotic electromagnetics methods, such as ray optics and physical optics, as well as full-wave numerical techniques, uncertainty quantification, surrogate models, and adjoint solutions.

JAKE J. HARMON (Member, IEEE) received the B.S. degree (summa cum laude) and the Ph.D. degree in electrical engineering from Colorado State University, Fort Collins, CO, USA, in 2019 and 2022, respectively.

He was with the Electromagnetics Laboratory, Colorado State University. He is currently a Postdoctoral Researcher with the Theoretical Division, Applied Mathematics and Plasma Physics Group, and the Center for Nonlinear Studies, Los Alamos National Laboratory. His Ph.D. research which was supported by the DoD High Performance Computing and Modernization Program and the U.S. Air Force Research Laboratory, was on the topics of adaptive numerical methods and uncertainty quantification, including goal-oriented error estimation and adaptivity, hp-refinement, and expediting the propagation of uncertainty in computational electromagnetics. His research interests include adaptive numerical methods, uncertainty quantification, and scientific computing.

BRANISLAV M. NOTAROŠ (Fellow, IEEE) received the Dipl.Ing. (B.S.), M.S., and Ph.D. degrees in electrical engineering from the University of Belgrade, Belgrade, Yugoslavia, in 1988, 1992, and 1995, respectively.

From 1996 to 1999, he was Assistant Professor with the School of Electrical Engineering, University of Belgrade. He was an Assistant and an Associate Professor with the Department of Electrical and Computer Engineering, University of Massachusetts Dartmouth from 1999 to 2006. He is currently a Professor of Electrical and Computer Engineering, the University Distinguished Teaching Scholar, and the Director of Electromagnetics Laboratory, Colorado State University. His publications include more than 300 journal and conference papers, and textbooks *Electromagnetics* (Pearson Prentice Hall, 2010) and *MATLAB-Based Electromagnetics* (Pearson Prentice Hall, 2013), and *Conceptual Electromagnetics* (CRC Press, 2017). His research contributions are in computational and applied electromagnetics. He was the recipient of the 1999 IEE Marconi Premium, the 2005 IEEE MTT-S Microwave Prize, the IEEE Antennas and Propagation Edward E. Altshuler Prize Paper Award in 2022, the ACES Technical Achievement Award in 2019, the Carnegie Foundation Colorado Professor of the Year Award in 2014, the ASEE ECE Distinguished Educator Award in 2015, the IEEE Undergraduate Teaching Award in 2015, and many other research and teaching awards. He serves as the President of the IEEE Antennas and Propagation Society (AP-S), the Immediate Past President of the Applied Computational Electromagnetics Society (ACES), the Immediate Past Chair of the USNC-URSI Commission B, and a Track Editor of the IEEE TRANSACTIONS ON ANTENNAS AND PROPAGATION. He served as the General Chair of the IEEE APS/URSI 2022 Denver Conference, the Chair of the IEEE AP-S Meetings Committee, the Chair of the Joint Meetings Committee, and an AP-S AdCom Member. He is Fellow of ACES.